Available online at www.sciencedirect.com

ScienceDirect

International Journal of Solids and Structures 44 (2007) 6318–6329

INTERNATIONAL JOURNAL OF SOLIDS AND STRUCTURES

www.elsevier.com/locate/ijsolstr

Tilting analysis of circular elastic layers interleaving with flexible reinforcements

Hsiang-Chuan Tsai *

Department of Construction Engineering, National Taiwan University of Science and Technology, P.O. Box 90-130, Taipei 106, Taiwan

Received 30 September 2006; received in revised form 14 February 2007
Available online 20 February 2007

Abstract

Bonding with reinforcements can increase the stiffness of elastic layers in the normal direction. The flexibility effect of the reinforcement on the bonded elastic layers of a circular cross-section subjected to pure bending moment is analyzed through a theoretical approach. Based on two kinematics assumptions in the elastic layers, the closed-form solutions of the horizontal displacements in the elastic layers and the reinforcements are solved using the governing equations established by stress equilibrium in the elastic layers and the reinforcements. Through these solved displacements, the tilting stiffness of the bonded elastic layer, the shear stress on the bonding surfaces, and the internal forces of the reinforcements are derived in closed forms.

Keywords: Bonded elastic layer; Elastomeric bearing; Seismic isolation

1. Introduction

A laminated elastomeric bearing consists of elastomeric layers bonded to interleaving reinforcing sheets. High stiffness of reinforcements restrains the lateral expansion of elastomeric layers and results in higher stiffness than an unbonded elastomeric layer in the vertical direction normal to the layer. By this characteristic, a laminated elastomeric bearing can provide high vertical rigidity to sustain gravity loading, while still providing the same horizontal flexibility of an unbonded elastomer.

To determine the compression stiffness of the bearing under vertical force and the tilting stiffness of the bearing under over-turning moment, the deformation of a single elastomeric layer bonded between reinforcements is analyzed. For the steel-reinforced bearings, the reinforcements can be assumed to be completely rigid. The compression stiffness and tilting stiffness of a single elastomeric layer bonded between two rigid plates have been derived for different shapes of bearings. The simplest approach to solve the stiffness is by assuming the elastomeric layer is an incompressible material (Gent and Lindley, 1959; Gent and Meinecke, 1970; Kelly, 1997). For nearly incompressible materials, such as rubber, the assumption of complete incompressibility

* Fax: +8862 27376606.
E-mail address: hctsai@mail.ntust.edu.tw

0020-7683/$ - see front matter
doi:10.1016/j.ijsolstr.2007.02.028

tends to overestimate the compression stiffness and tilting stiffness of the bonded rubber layer when the shape factor of the bonded layer (defined as the ratio of the one bonded area to the force-free area) is high. Including the effect of bulk compressibility can overcome this problem (Chalhoub and Kelly, 1990, 1991; Kelly, 1997). For the compressible elastic layers, there are several stiffness solutions for different shapes of the bearings (Lindley, 1979a,b, Koh and Kelly, 1989; Koh and Lim, 2001; Tsai, 2003, 2005; Tsai and Lee, 1998, 1999). These solutions are suitable for materials of any Poisson's ratio.

For some laminated elastomeric bearings, such as fiber-reinforced bearings, the reinforcements still have high stiffness but cannot be assumed to be completely rigid. The in-plane stiffness of the reinforcements must be considered in the analysis. The compression stiffness and the tilting stiffness of the bearings with incompressible layers and flexible reinforcements are derived for different shapes (Kelly, 1999; Tsai and Kelly, 2001, 2002a,b). For the nearly incompressible elastomeric layers, bulk compressibility is included in the stiffness analysis of fiber-reinforced bearings of the infinite-strip shape (Kelly, 2002; Kelly and Takhirov, 2002). Recently, the compression stiffness of the bearings with compressible elastic layers of any Poisson's ratio and flexible reinforcements is derived for the infinite-strip shape (Tsai, 2004) and the circular shape (Tsai, 2006).

Tilting analyses of circular bearings have been carried out by Tsai and Kelly (2002b), where the elastic layer is incompressible and the reinforcement is flexible, and by Tsai (2003), where the elastic layer is compressible but the reinforcement is rigid. In this paper, the tilting stiffness of the circular bearings with compressible elastic layers and flexible reinforcements is derived. The elastic layers adopt two kinematics assumptions: (i) planes parallel to the reinforcements before deformation remain planar after loading; (ii) lines normal to the reinforcements before deformation become parabolic after loading. The flexible reinforcements in the bearing are assumed to have the same deformation, which implies that every elastic layer in the bearing has the same tilting stiffness, so only a single elastic layer bonding with flexible reinforcements is analyzed.

2. Governing equations

Fig. 1 shows an elastic layer in a circular bearing, which has a diameter of $2b$ and a thickness of t. Its top and bottom surfaces are perfectly bonded to flexible reinforcements of thickness of t_f. When a pure bending moment M is applied to the top and bottom reinforcements that are assumed to remain planar, the two reinforcements rotate about the y axis and form an angle ϕ. A cylindrical coordinate system (r, θ, z) is established with the origin at the center of the layer, so that the angle ϕ is symmetric to the $r-\theta$ plane at $z=0$. Denote u, v and w as the displacements of the elastic layer along the r, θ and z directions, respectively, which are assumed to have the form

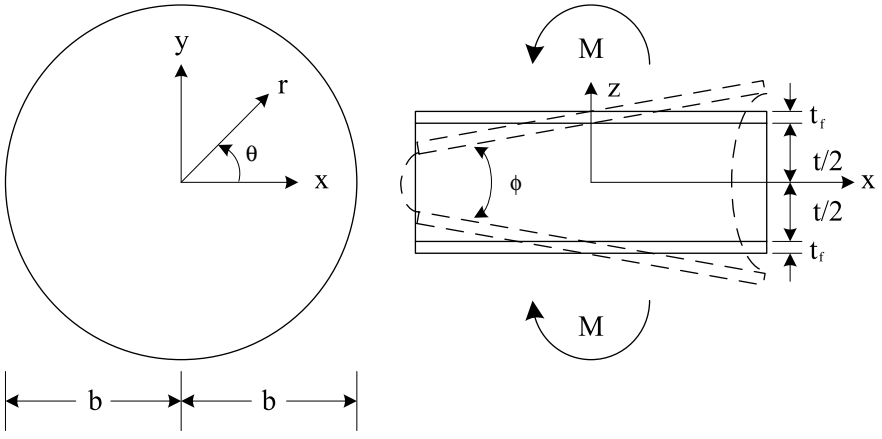

Fig. 1. Circular elastic layer bonded between reinforcements under flexure load.

$$u(r,\theta,z) = u_0(r,\theta)\left(1-\frac{4z^2}{t^2}\right) + u_1(r,\theta) \tag{1}$$

$$v(r,\theta,z) = v_0(r,\theta)\left(1-\frac{4z^2}{t^2}\right) + v_1(r,\theta) \tag{2}$$

$$w(r,\theta,z) = \frac{1}{\rho} zr\cos\theta \tag{3}$$

where $\rho = t/\phi$ is the radius of bending curvature. In Eqs. (1) and (2), the terms of u_0 and v_0 represent the kinematics assumption of quadratic-varied displacements and are supplemented by additional displacement u_1 and v_1, respectively, which are constant through the thickness and are intended to accommodate the stretch of the reinforcement. Eq. (3) represents the assumption that planes parallel to the reinforcements remain planar.

For clarification, the following displacement functions are defined

$$f_0(r,\theta) = u_{0,r} + \frac{u_0}{r} + \frac{v_{0,\theta}}{r} \tag{4}$$

$$f_1(r,\theta) = u_{1,r} + \frac{u_1}{r} + \frac{v_{1,\theta}}{r} \tag{5}$$

$$g_0(r,\theta) = v_{0,r} + \frac{v_0}{r} - \frac{u_{0,\theta}}{r} \tag{6}$$

$$g_1(r,\theta) = v_{1,r} + \frac{v_1}{r} - \frac{u_{1,\theta}}{r} \tag{7}$$

Substituting the displacement assumption into the equilibrium equations of the elastic layer in the r and θ directions and integrating the resulting equations through the thickness of the layer leads to

$$u_0 = \frac{8}{t^2}\left[\frac{2(1-v)}{(1-2v)}\left(\frac{2}{3}f_{0,r} + f_{1,r}\right) - \left(\frac{2}{3}\frac{g_{0,\theta}}{r} + \frac{g_{1,\theta}}{r}\right) + \frac{1}{\rho(1-2v)}\cos\theta\right] \tag{8}$$

$$v_0 = \frac{8}{t^2}\left[\frac{2(1-v)}{(1-2v)}\left(\frac{2}{3}\frac{f_{0,\theta}}{r} + \frac{f_{1,\theta}}{r}\right) + \left(\frac{2}{3}g_{0,r} + g_{1,r}\right) - \frac{1}{\rho(1-2v)}\sin\theta\right] \tag{9}$$

in which v is Poisson's ratio of the elastic layer. Differentiating the multiplication of r and Eq. (8) with respect to r and then adding the result to the differentiation of Eq. (9) with respect to θ gives

$$\frac{2}{3}\left(f_{0,rr} + \frac{f_{0,r}}{r} + \frac{f_{0,\theta\theta}}{r^2} - \frac{6(1-2v)}{t^2(1-v)}f_0\right) + \left(f_{1,rr} + \frac{f_{1,r}}{r} + \frac{f_{1,\theta\theta}}{r^2}\right) = 0 \tag{10}$$

Differentiating the multiplication of r and Eq. (9) with respect to r and then subtracting the result from the differentiation of Eq. (8) with respect to θ gives

$$\frac{2}{3}\left(g_{0,rr} + \frac{g_{0,r}}{r} + \frac{g_{0,\theta\theta}}{r^2} - \frac{12}{t^2}g_0\right) + \left(g_{1,rr} + \frac{g_{1,r}}{r} + \frac{g_{1,\theta\theta}}{r^2}\right) = 0 \tag{11}$$

The thickness of the reinforcements is much smaller than the thickness of the elastic layers, so that the normal and shear forces per unit length in the reinforcement, N_{rr}, $N_{\theta\theta}$ and $N_{r\theta}$, can be established by the plane-stress formulae (Tsai and Kelly, 2002b). The equilibrium equations of the reinforcement in the r and θ directions (Tsai and Kelly, 2002b) become

$$f_{1,r} - \left(\frac{1-v_f}{2}\right)\frac{g_{1,\theta}}{r} = -\gamma\frac{(1-v_f^2)}{2(1+v)}\left(\frac{8}{t^2}u_0 - \frac{1}{\rho}\cos\theta\right) \tag{12}$$

$$\frac{f_{1,\theta}}{r} + \left(\frac{1-v_f}{2}\right)g_{1,r} = -\gamma\frac{(1-v_f^2)}{2(1+v)}\left(\frac{8}{t^2}v_0 + \frac{1}{\rho}\sin\theta\right) \tag{13}$$

where v_f is the Poisson's ratio of the reinforcement and γ is the stiffness ratio between the elastic layer and the reinforcement, defined as

$$\gamma = \frac{Et}{E_f t_f} \tag{14}$$

with E and E_f being the elastic modulus of the elastic layer and the reinforcement, respectively.

Differentiating the multiplication of r and Eq. (12) with respect to r and then adding the result to the differentiation of Eq. (13) with respect to θ yields

$$f_{1,rr}+\frac{f_{1,r}}{r}+\frac{f_{1,\theta\theta}}{r^2}=-\gamma\frac{4(1-v_f^2)}{t^2(1+v)}f_0 \tag{15}$$

Differentiating the multiplication of r and Eq. (13) with respect to r and then subtracting the result from the differentiation of Eq. (12) with respect to θ yields

$$g_{1,rr}+\frac{g_{1,r}}{r}+\frac{g_{1,\theta\theta}}{r^2}=-\gamma\frac{8(1+v_f)}{t^2(1+v)}g_0 \tag{16}$$

Substituting Eqs. (15) and (16) into Eqs. (10) and (11), respectively, gives

$$f_{0,rr}+\frac{f_{0,r}}{r}+\frac{f_{0,\theta\theta}}{r^2}-\alpha^2 f_0=0 \tag{17}$$

$$g_{0,rr}+\frac{g_{0,r}}{r}+\frac{g_{0,\theta\theta}}{r^2}-\beta^2 g_0=0 \tag{18}$$

where α is defined as

$$\alpha=\sqrt{\frac{6}{t^2}\left(\frac{1-2v}{1-v}+\frac{1-v_f^2}{1+v}\gamma\right)} \tag{19}$$

and β is defined as

$$\beta=\sqrt{\frac{12}{t^2}\left(1+\frac{1+v_f}{1+v}\gamma\right)} \tag{20}$$

3. Solution of displacements

The deformation of the elastic layer has the symmetric and anti-symmetric properties as

$$u(r,\theta,z)=u(r,-\theta,z)=-u(r,\pi-\theta,z) \tag{21}$$

$$v(r,\theta,z)=-v(r,-\theta,z)=v(r,\pi-\theta,z) \tag{22}$$

To satisfy the above conditions, the solutions of Eqs. (17) and (18) have the forms

$$f_0(r,\theta)=\frac{b}{\rho}\sum_{n=1,3,5,\ldots}^{\infty}A_n I_n(\alpha r)\cos n\theta \tag{23}$$

$$g_0(r,\theta)=\frac{b}{\rho}\sum_{n=1,3,5,\ldots}^{\infty}B_n I_n(\beta r)\sin n\theta \tag{24}$$

where I_n is the modified Bessel function of the first kind of order n; A_n and B_n are the constants to be determined.

Substituting Eqs. (23) and (24) into Eqs. (15) and (16), respectively, gives the solutions

$$f_1(r,\theta)=\frac{b}{\rho}\sum_{n=1,3,5,\ldots}^{\infty}\left(\frac{1}{b}C_n r^n-\overline{\alpha}A_n I_n(\alpha r)\right)\cos n\theta \tag{25}$$

$$g_1(r,\theta)=\frac{b}{\rho}\sum_{n=1,3,5,\ldots}^{\infty}\left(\frac{1}{b}D_n r^n-\overline{\beta}B_n I_n(\beta r)\right)\sin n\theta \tag{26}$$

where C_n and D_n are the constants to be determined, $\overline{\alpha}$ is defined as

$$\overline{\alpha} = \frac{2(1-v)(1-v_f^2)\gamma}{3[(1-v)(1-v_f^2)\gamma + (1-2v)(1+v)]} \tag{27}$$

and $\overline{\beta}$ is defined as

$$\overline{\beta} = \frac{2(1+v_f)\gamma}{3[(1+v_f)\gamma + (1+v)]} \tag{28}$$

Substituting Eq. (8) into Eq. (12) and using the solutions in Eqs. (23)–(26) leads to

$$D_1 = \frac{2(1-v)\overline{\beta}}{(1-2v)\overline{\alpha}} C_1 + \frac{3v\overline{\beta}}{(1-2v)} \tag{29}$$

and, for $n = 3,5,7,\ldots,\infty$,

$$D_n = \frac{2(1-v)\overline{\beta}}{(1-2v)\overline{\alpha}} C_n \tag{30}$$

Substituting Eq. (9) into Eq. (13) obtains the same results as Eqs. (29) and (30).

The solutions displayed in Eqs. (25) and (26) indicate the displacements of the reinforcement can be expressed as

$$u_1(r,\theta) = \sum_{n=1,3,5,\ldots}^{\infty} u_1^{(n)}(r)\cos n\theta \tag{31}$$

$$v_1(r,\theta) = \sum_{n=1,3,5,\ldots}^{\infty} v_1^{(n)}(r)\sin n\theta \tag{32}$$

where $u_1^{(n)}$ and $v_1^{(n)}$ represent the amplitudes of the nth term in u_1 and v_1, respectively. Substituting the above equations into Eqs. (5) and (7) and applying the solutions in Eqs. (25) and (26) leads to

$$u_{1,r}^{(n)} + \frac{1}{r}u_1^{(n)} + \frac{n}{r}v_1^{(n)} = \frac{1}{\rho}C_n r^n - \frac{b}{\rho}\overline{\alpha}A_n I_n(\alpha r) \tag{33}$$

$$v_{1,r}^{(n)} + \frac{1}{r}v_1^{(n)} + \frac{n}{r}u_1^{(n)} = \frac{1}{\rho}D_n r^n - \frac{b}{\rho}\overline{\beta}B_n I_n(\beta r) \tag{34}$$

The summation of Eq. (33) with Eq. (34) and the subtraction of Eq. (33) from Eq. (34) results in the solutions of $u_1^{(n)} + v_1^{(n)}$ and $u_1^{(n)} - v_1^{(n)}$, respectively. Combining these results yields

$$\begin{aligned} u_1^{(n)} = {} & -\frac{b}{\rho}A_n\frac{\overline{\alpha}}{2\alpha}[I_{n+1}(\alpha r) + I_{n-1}(\alpha r)] - \frac{b}{\rho}B_n\frac{\overline{\beta}}{2\beta}[I_{n+1}(\beta r) - I_{n-1}(\beta r)] \\ & + \frac{1}{\rho}C_n\frac{n+2}{4(n+1)}r^{n+1} - \frac{1}{\rho}D_n\frac{n}{4(n+1)}r^{n+1} + \frac{b^2}{\rho}F_n\frac{1}{2}r^{n-1} \end{aligned} \tag{35}$$

$$\begin{aligned} v_1^{(n)} = {} & -\frac{b}{\rho}A_n\frac{\overline{\alpha}}{2\alpha}[I_{n+1}(\alpha r) - I_{n-1}(\alpha r)] - \frac{b}{\rho}B_n\frac{\overline{\beta}}{2\beta}[I_{n+1}(\beta r) + I_{n-1}(\beta r)] \\ & - \frac{1}{\rho}C_n\frac{n}{4(n+1)}r^{n+1} + \frac{1}{\rho}D_n\frac{n+2}{4(n+1)}r^{n+1} - \frac{b^2}{\rho}F_n\frac{1}{2}r^{n-1} \end{aligned} \tag{36}$$

where F_n is an integration constant.

The normal force and shear force of the reinforcement vanish at the edge $r = b$

$$N_{rr}(b,\theta) = 0, N_{r\theta}(b,\theta) = 0 \tag{37}$$

which implies

$$f_1(b,\theta)-(1-v_f)\left(\frac{1}{b}u_1(b,\theta)+\frac{1}{b}v_{1,\theta}(b,\theta)\right)=0 \tag{38}$$

$$g_1(b,\theta)+\frac{2}{b}u_{1,\theta}(b,\theta)-\frac{2}{b}v_1(b,\theta)=0 \tag{39}$$

The normal stress and shear stress of the elastic layer vanish at the edge $r=b$

$$\sigma_{rr}(b,\theta,z)=0,\quad \tau_{r\theta}(b,\theta,z)=0 \tag{40}$$

Integrating the above equations through the thickness of the elastic layer and using Eqs. (38) and (39) leads to

$$\left(\frac{1-v}{1-2v}\right)\frac{2}{3}f_0(b,\theta)+\left(\frac{v}{1-2v}-\frac{v_f}{1-v_f}\right)f_1(b,\theta)-\frac{2}{3}\left(\frac{u_0(b,\theta)}{b}+\frac{v_0(b,\theta)}{b}\right)+\left(\frac{v}{1-2v}\right)\frac{b}{\rho}\cos\theta=0 \tag{41}$$

$$g_0(b,\theta)+\frac{2}{b}u_{0,\theta}(b,\theta)-\frac{2}{b}v_0(b,\theta)=0 \tag{42}$$

The constants for $n=1$ can be solved from Eqs. (38), (39), (41) and (42) as

$$A_1=-\frac{v}{\Lambda}\left(\frac{\beta bI_1(\beta b)}{2I_2(\beta b)}-1\right)\frac{\alpha b}{I_2(\alpha b)} \tag{43}$$

$$B_1=-\frac{v}{\Lambda}\frac{\beta b}{I_2(\beta b)} \tag{44}$$

$$C_1=-\frac{v}{\Lambda}\left[\overline{\alpha}\left(\frac{(1-v_f)}{(1+v_f)}\frac{\alpha bI_3(\alpha b)}{I_2(\alpha b)}+\frac{\alpha bI_1(\alpha b)}{I_2(\alpha b)}\right)\left(\frac{\beta bI_1(\beta b)}{2I_2(\beta b)}-1\right)+\overline{\beta}\frac{(1-v_f)}{(1+v_f)}\frac{\beta bI_3(\beta b)}{I_2(\beta b)}\right] \tag{45}$$

$$D_1=-\frac{v}{\Lambda}\left[\overline{\alpha}\frac{2}{(1+v_f)}\frac{\alpha bI_3(\alpha b)}{I_2(\alpha b)}\left(\frac{\beta bI_1(\beta b)}{2I_2(\beta b)}-1\right)+\overline{\beta}\left(\frac{2}{(1+v_f)}\frac{\beta bI_3(\beta b)}{I_2(\beta b)}+\frac{\beta bI_1(\beta b)}{I_2(\beta b)}\right)\right] \tag{46}$$

with

$$\begin{aligned}\Lambda=&\left[\left(v-\frac{v_f}{1+v_f}\right)\overline{\alpha}\frac{\alpha bI_3(\alpha b)}{I_2(\alpha b)}+\frac{2(1-v)}{3}\frac{\alpha bI_1(\alpha b)}{I_2(\alpha b)}\right]\left(\frac{\beta bI_1(\beta b)}{2I_2(\beta b)}-1\right)\\&+\left[\left(v-\frac{v_f}{1+v_f}\right)\overline{\beta}\frac{\beta bI_3(\beta b)}{I_2(\beta b)}-\frac{(1-2v)}{3}\frac{\beta bI_1(\beta b)}{I_2(\beta b)}\right]\end{aligned} \tag{47}$$

The constants for $n=3,5,7,\ldots$ solved from Eqs. (30), (38), (39), (41) and (42) are found as

$$A_n=B_n=C_n=D_n=F_n=0 \tag{48}$$

which means that the displacements of the elastic layer and the reinforcement are proportional to $\cos\theta$ or $\sin\theta$, and do not contain any higher term of Fourier series. The C_1 and D_1 solutions in Eqs. (45) and (46) are not derived from Eq. (29) but can satisfy Eq. (29). The constant F_1 is solved by setting $u_1=v_1=0$ at $r=0$, that is, $u_1^{(1)}(0,\theta)=v_1^{(1)}(0,\theta)=0$ in Eqs. (35) and (36), which gives

$$F_1=\frac{\overline{\alpha}}{\alpha b}A_1-\frac{\overline{\beta}}{\beta b}B_1 \tag{49}$$

From Eqs. (8) and (9), the solution of the displacements in the elastic layer becomes

$$u_0=\frac{b^2}{\rho}\left[A_1\frac{1}{\alpha b}\left(I_0(\alpha r)-\frac{I_1(\alpha r)}{\alpha r}\right)-B_1\frac{1}{\beta b}\frac{I_1(\beta r)}{\beta r}+\frac{1}{32S^2}\left(C_1\frac{2(1-v)}{1-2v}-D_1+\frac{1}{1-2v}\right)\right]\cos\theta \tag{50}$$

$$v_0=-\frac{b^2}{\rho}\left[A_1\frac{1}{\alpha b}\frac{I_1(\alpha r)}{\alpha r}-B_1\frac{1}{\beta b}\left(I_0(\beta r)-\frac{I_1(\beta r)}{\beta r}\right)+\frac{1}{32S^2}\left(C_1\frac{2(1-v)}{1-2v}-D_1+\frac{1}{1-2v}\right)\right]\sin\theta \tag{51}$$

in which

$$S=\frac{b}{2t} \tag{52}$$

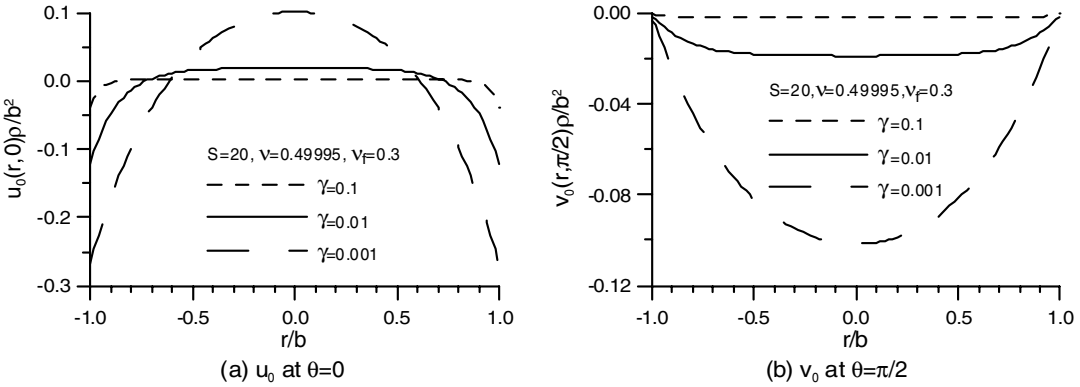

Fig. 2. Displacement functions u_0 and v_0 varied with radial distance.

is the shape factor of the bonded circular layers. From Eqs. (35) and (36), the solution of the reinforcement displacements becomes

$$u_1 = \frac{b^2}{\rho}\left[A_1\frac{\overline{\alpha}}{2\alpha b}[1 - I_2(\alpha r) - I_0(\alpha r)] + B_1\frac{\overline{\beta}}{2\beta b}[-1 - I_2(\beta r) + I_0(\beta r)] + \left(\frac{3}{8}C_1 - \frac{1}{8}D_1\right)\frac{r^2}{b^2}\right]\cos\theta \tag{53}$$

$$v_1 = \frac{b^2}{\rho}\left[A_1\frac{\overline{\alpha}}{2\alpha b}[-1 - I_2(\alpha r) + I_0(\alpha r)] + B_1\frac{\overline{\beta}}{2\beta b}[1 - I_2(\beta r) + I_0(\beta r)] + \left(-\frac{1}{8}C_1 + \frac{3}{8}D_1\right)\frac{r^2}{b^2}\right]\sin\theta \tag{54}$$

The displacement functions u_0 and v_0 represent the bulge deformation in the elastic layers, which are plotted in Fig. 2 as functions of r/b for $S = 20$, $v = 0.49995$, $v_f = 0.3$ and several stiffness ratios γ. The figure shows that the elastic layer bonded with the reinforcements of higher stiffness has larger bulge deformation. The reinforcement displacements u_1 and v_1 are plotted in Fig. 3 as functions of r/b for $S = 20$, $v = 0.49995$, $v_f = 0.3$ and several stiffness ratios γ, which indicate that the reinforcement has less deformation for the reinforcements of higher stiffness. The radial displacement u_1 of $\gamma = 0.01$ is very close to that of $\gamma = 0.001$ in the center part, but has an obvious difference near the edge.

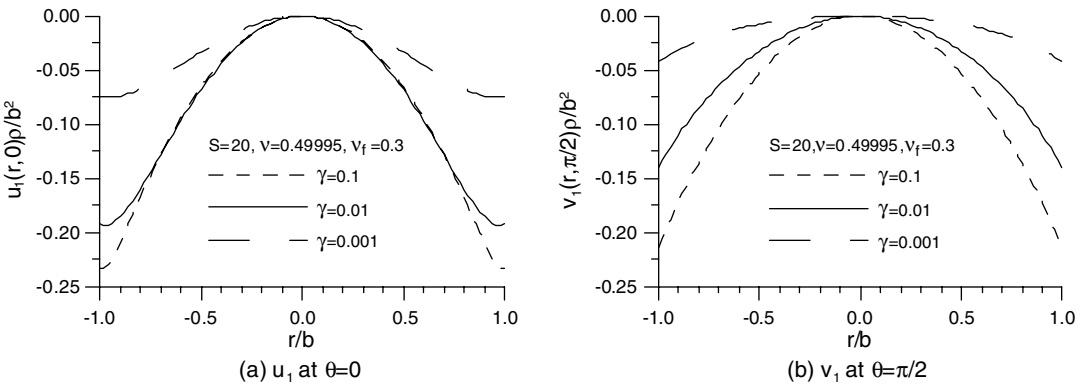

Fig. 3. Reinforcement displacements u_1 and v_1 varied with radial distance.

4. Tilting stiffness

According to beam theory, the effective tilting stiffness of the elastic layer is defined as

$$(EI)_{\text{eff}} = \rho \int_0^{2\pi} \int_0^b \overline{\sigma}_{zz} r^2 \cos\theta \, \mathrm{d}r \, \mathrm{d}\theta \tag{55}$$

in which $\overline{\sigma}_{zz}$ is the effective vertical stress defined as

$$\overline{\sigma}_{zz} = \frac{1}{t} \int_{-t/2}^{t/2} \sigma_{zz} \, \mathrm{d}z \tag{56}$$

By using the displacement solution in the last section, the effective vertical stress can be derived as

$$\overline{\sigma}_{zz} = \frac{b}{\rho} E \left[\left(\frac{v}{(1-2v)(1+v) + (1-v)(1-v_{\text{f}}^2)\gamma} \right) \frac{2}{3} A_1 I_1(\alpha r) + \frac{v}{(1-2v)(1+v)} \left(\frac{1-v}{v} + C_1 \right) \frac{r}{b} \right] \cos\theta \tag{57}$$

For clarification, define the effective bending modulus as $E_b = (EI)_{\text{eff}}/I_r$ where $I_r = \pi b^4/4$ is the moment of inertia of the circular area about the r axis. Substituting Eq. (57) into Eq. (55), the effective bending modulus can be derived as

$$\frac{E_b}{E} = \frac{1}{1+v} + \frac{v}{(1+v)(1-2v)} \left\{ 1 - \frac{v}{\Lambda} \left[\frac{(1-v_{\text{f}})}{(1+v_{\text{f}})} \overline{\beta} \frac{\beta b I_3(\beta b)}{I_2(\beta b)} + \left(\frac{1}{(1+v_{\text{f}})} \overline{\alpha} \frac{\alpha b I_3(\alpha b)}{I_2(\alpha b)} + \frac{4}{3} \right) \left(\frac{\beta b I_1(\beta b)}{I_2(\beta b)} - 2 \right) \right] \right\} \tag{58}$$

When γ tends to zero, the reinforcement becomes rigid; Eqs. (27) and (28) gives $\overline{\alpha} = \overline{\beta} = 0$. By assigning these values to Eq. (58), we can obtain the same solution as Tsai (2003) for the tilting stiffness of circular layers bonded to the rigid reinforcements. When Poisson's ratio $v \to 0.5$, the asymptotic solution of Eq. (58) is

$$\frac{E_b}{E} = \frac{4}{3} + \frac{1}{3\Lambda_0} \left[\left(\frac{24S^2}{(\alpha_0 b)^2} - \frac{1}{(1+v_{\text{f}})} \right) \left(\frac{\beta_0 b I_1(\beta_0 b)}{I_2(\beta_0 b)} - 2 \right) \frac{\alpha_0 b I_3(\alpha_0 b)}{I_2(\alpha_0 b)} - \left(\frac{3}{(1+v_{\text{f}})} \overline{\beta}_0 \frac{\beta_0 b I_3(\beta_0 b)}{I_2(\beta_0 b)} + \frac{\beta_0 b I_1(\beta_0 b)}{I_2(\beta_0 b)} \right) \right] \tag{59}$$

in which

$$\Lambda_0 = \left(\frac{\beta_0 b I_1(\beta_0 b)}{I_2(\beta_0 b)} - 2 \right) \left(\frac{1}{(1+v_{\text{f}})} \frac{\alpha_0 b I_3(\alpha_0 b)}{I_2(\alpha_0 b)} + 2 \right) + \frac{3(1-v_{\text{f}})}{2(1+v_{\text{f}})} \overline{\beta}_0 \frac{\beta_0 b I_3(\beta_0 b)}{I_2(\beta_0 b)} \tag{60}$$

$$\alpha_0 b = 4S\sqrt{(1-v_{\text{f}}^2)\gamma} \tag{61}$$

$$\beta_0 b = 4S\sqrt{3 + 2(1+v_{\text{f}})\gamma} \tag{62}$$

$$\overline{\beta}_0 = \frac{2}{3} \left(\frac{2(1+v_{\text{f}})\gamma}{3 + 2(1+v_{\text{f}})\gamma} \right) \tag{63}$$

This is the effective bending modulus of the circular layers of incompressible materials interleaving with flexible reinforcements.

The curves of the bending modulus calculated from Eq. (58) for $S = 2$ and $S = 20$ are plotted as a function of v in Fig. 4 and as a function of γ in Fig. 5, which indicate that the bending modulus increases with increasing the Poisson's ratio of the elastic layer or the stiffness of the reinforcement. For the high shape factor ($S = 20$), the bending modulus dramatically increases when v is close to 0.5 and γ is close to 0. The solutions of the finite element method are also plotted in Fig. 4. The finite element model is a bearing of 20 elastic layers. Both ends of the bearing are free for the lateral deformation. The theoretical solution derived in this paper assumes every sheet of reinforcement in the bearing has the same deformation, which means that the boundary effect at the ends of the bearing is neglected and the ideal model of the theoretical solution is a bearing having an infinite number of elastic layers. Therefore, the finite element solutions have slight deviation from the theoretical solutions. In Fig. 5(b), the bending modules calculated from Eq. (59) for the incompressible elastic layers

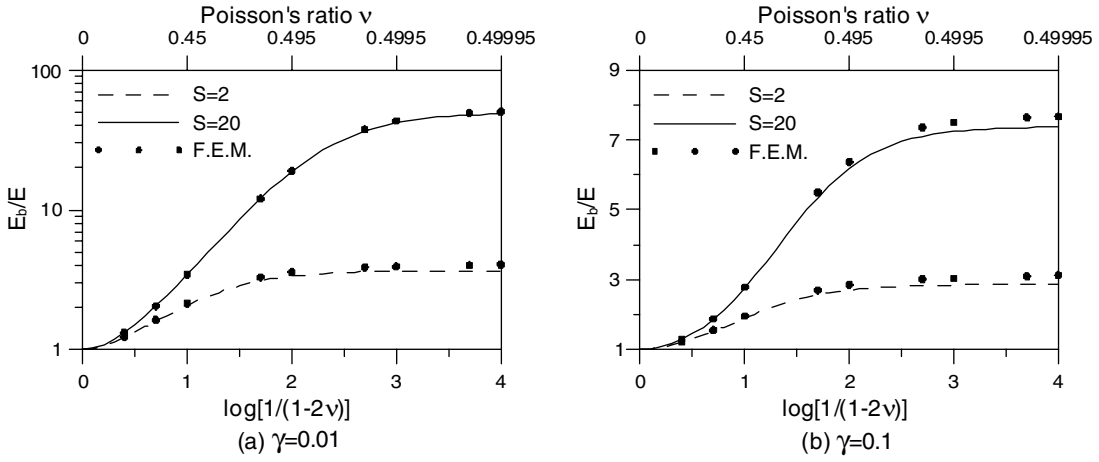

Fig. 4. Effective bending modulus varied with Poisson's ratio ($v_f = 0.3$).

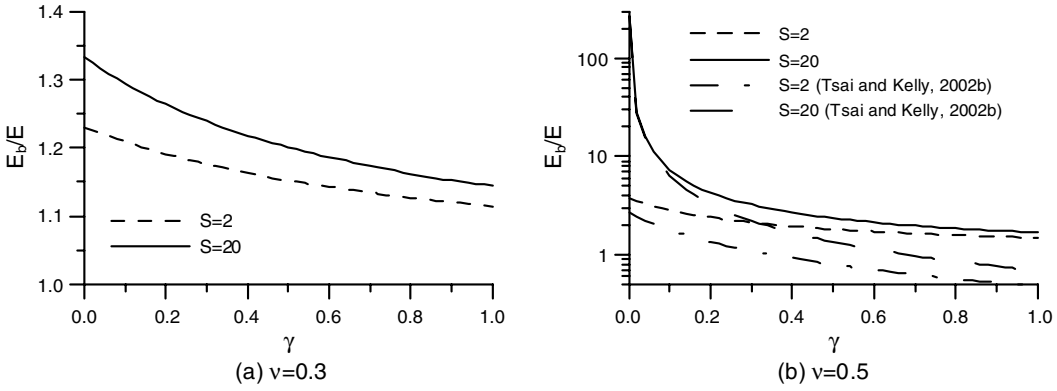

Fig. 5. Effective bending modulus varied with stiffness ratio ($v_f = 0.3$).

are compared with the solutions by Tsai and Kelly (2002b), which indicates that the solution by Tsai and Kelly (2002b) is applicable only when the shape factor is high and the stiffness ratio is low.

5. Stress distribution

The shear stresses in the bonding surface between the elastic layer and the reinforcement, $\tau_{rz}(r,\theta,t/2)$ and $\tau_{\theta z}(r,\theta,t/2)$, can be derived by using Eqs. (50) and (51), respectively. The bonding shear stress in the radial direction at $\theta = 0$ and the bonding shear stress in the tangential direction at $\theta = \pi/2$ are plotted in Fig. 6 as functions of r/b for $S = 20$, $v = 0.49995$, $v_f = 0.3$ and several stiffness ratios γ, which indicates that, for the elastic layer bonded with the reinforcements of lower stiffness, the bonding shear stress in the radial direction increases more sharply near the boundary, and the bonding shear stress in the tangential direction distributes more uniformly over the central part.

Using the reinforcement displacements in Eqs. (53) and (54), the in-plane force components in the reinforcement are

$$N_{rr} = \frac{b}{\rho}\frac{E_f t_f}{(1+v_f)}\cos\theta\left\{-A_1\overline{\alpha}\left(\frac{1}{(1-v_f)}I_1(\alpha r) - \frac{I_2(\alpha r)}{\alpha r}\right) + B_1\overline{\beta}\frac{I_2(\beta r)}{\beta r} - \frac{v}{\Lambda}\left[\overline{\alpha}\left(\frac{\alpha b I_1(\alpha b)}{(1-v_f)I_2(\alpha b)} - 1\right)\left(\frac{\beta b I_1(\beta b)}{2I_2(\beta b)} - 1\right) - \overline{\beta}\right]\frac{r}{b}\right\} \tag{64}$$

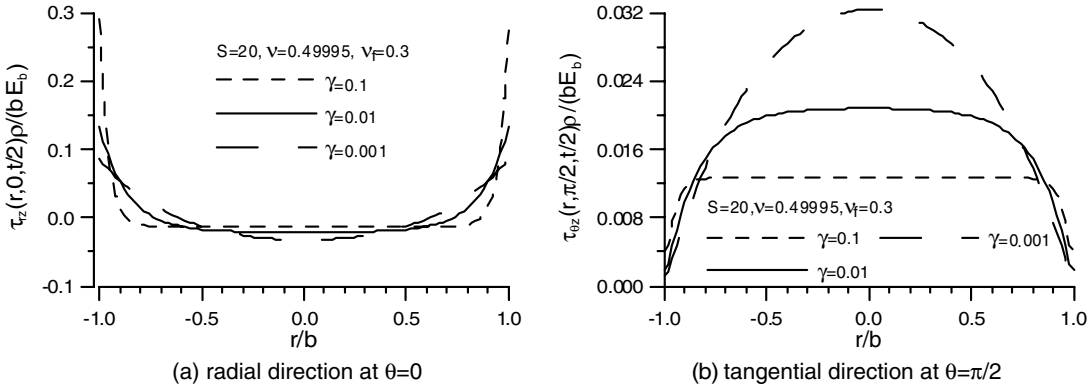

Fig. 6. Bonding shear stresses varied with radial distance.

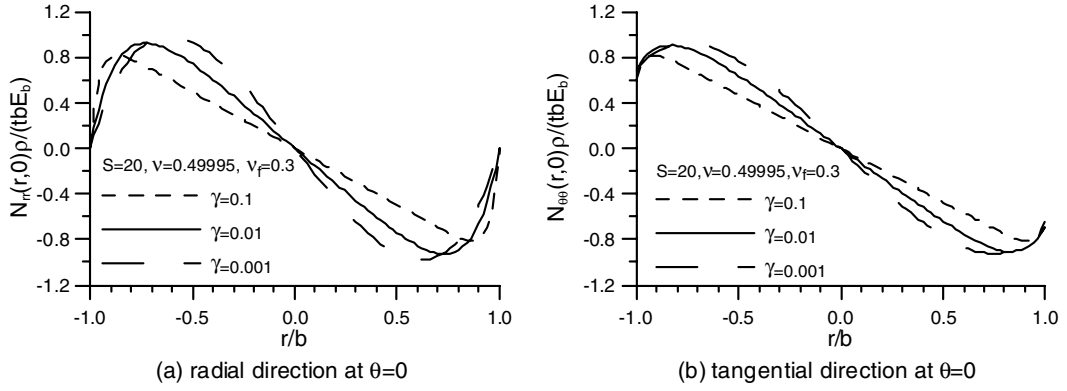

Fig. 7. Normal forces in reinforcements at $\theta = 0$ varied with radial distance.

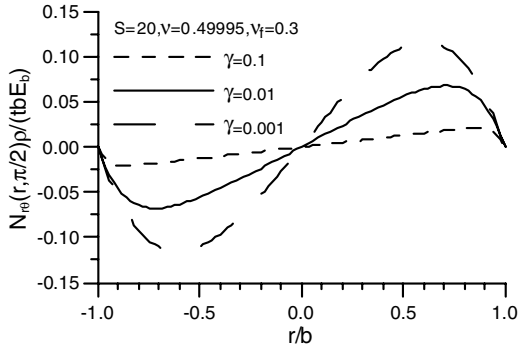

Fig. 8. Shear force in reinforcements at $\theta = \pi/2$ varied with radial distance.

$$N_{\theta\theta} = \frac{b}{\rho}\frac{E_f t_f}{(1+\nu_f)}\cos\theta\left\{-A_1\overline{\alpha}\left(\frac{\nu_f}{(1-\nu_f)}I_1(\alpha r)+\frac{I_2(\alpha r)}{\alpha r}\right)-B_1\overline{\beta}\frac{I_2(\beta r)}{\beta r}\right.$$
$$\left.-\frac{\nu}{\Lambda}\left[\overline{\alpha}\left(\frac{\alpha b I_1(\alpha b)}{(1-\nu_f)I_2(\alpha b)}-3\right)\left(\frac{\beta b I_1(\beta b)}{2I_2(\beta b)}-1\right)+\overline{\beta}\left(\frac{\beta b I_1(\beta b)}{I_2(\beta b)}-3\right)\right]\frac{r}{b}\right\} \tag{65}$$

$$N_{r\theta} = \frac{b}{\rho}\frac{E_f t_f}{(1+v_f)}\sin\theta\left[A_1\overline{\alpha}\frac{I_2(\alpha r)}{\alpha r} - B_1\overline{\beta}\left(\frac{1}{2}I_1(\beta r) - \frac{I_2(\beta r)}{\beta r}\right) - \frac{v}{\Lambda}(\overline{\beta}-\overline{\alpha})\left(\frac{\beta b I_1(\beta b)}{I_2(\beta b)} - 2\right)\frac{b}{r}\right] \tag{66}$$

The normal forces at $\theta = 0$ and the shear force at $\theta = \pi/2$ are plotted in Figs. 7 and 8, respectively, as functions of r/b for $S = 20$, $v = 0.49995$, $v_f = 0.3$ and several stiffness ratios γ, which indicate that, for the reinforcement of lower stiffness, the in-plane forces vary more linearly over the central part.

6. Conclusion

Based on the two kinematics assumptions, i.e. horizontal planes remain planar and vertical lines become parabolic after deformation, the circular elastic layers interleaving with flexible reinforcements are analyzed through a theoretical approach to find the closed-form solutions of horizontal displacements in the elastic layers and reinforcements under a pure bending moment, from which the tilting stiffness can be derived. The displacements in the radial and tangential directions are shown to be proportional to $\cos\theta$ and $\sin\theta$, respectively, and not contain any higher term of Fourier series. The analysis has no limitation on Poisson's ratio and the reinforcement stiffness, so that the effect of Poisson's ratio and the reinforcement stiffness can be studied. High tilting stiffness can be achieved by using high shape factor, high Poisson's ratio of the elastic layer and high stiffness of the reinforcement. For the elastic layers of incompressible material, the tilting stiffness is derived through the asymptotic approach, which provides more accurate solution. The solution of the previous research, by directly neglecting the bulk compressibility, is accurate only when the shape factor is large and the reinforcement stiffness is high. The reinforcement flexibility can also affect the shear stress distribution on the bonding surface between the elastic layer and the reinforcement. For the reinforcements of lower stiffness, the bonding shear stresses have sharper increase in the radial direction near the boundary, but have more uniform distribution in the tangential direction over the central part.

Acknowledgement

The National Science Council of Taiwan supported the research work reported in this paper under Grant No. NSC94-2211-E011-013. This support is greatly appreciated.

References

Chalhoub, M.S., Kelly, J.M., 1990. Effect of bulk compressibility on the stiffness of cylindrical base isolation bearings. International Journal of Solids and Structures 26, 734–760.

Chalhoub, M.S., Kelly, J.M., 1991. Analysis of infinite-strip-shaped base isolator with elastomer bulk compression. Journal of Engineering Mechanics, ASCE 117, 1791–1805.

Gent, A.N., Lindley, P.B., 1959. The compression of bonded rubber blocks. Proceeding of the Institution Mechanical Engineers 173, 111–117.

Gent, A.N., Meinecke, E.A., 1970. Compression, bending and shear of bonded rubber blocks. Polymer Engineering and Science 10, 48–53.

Kelly, J.M., 1997. Earthquake-Resistant Design with Rubber, second ed. Springer-Verlag, London.

Kelly, J.M., 1999. Analysis of fiber-reinforced elastomeric isolator. Journal of Seismology and Earthquake Engineering 2, 19–34.

Kelly, J.M., 2002. Seismic isolation systems for developing countries. Earthquake Spectra 18, 385–406.

Kelly, J.M., Takhirov, S.M., 2002. Analytical and experimental study of fiber-reinforced strip isolators. PEER Report 2002/11, Pacific Earthquake Engineering Research Center, University of California, Berkeley.

Koh, C.G., Kelly, J.M., 1989. Compression stiffness of bonded square layers of nearly incompressible material. Engineering Structures 11, 9–15.

Koh, C.G., Lim, H.L., 2001. Analytical solution for compression stiffness of bonded rectangular layers. International Journal of Solids and Structures 38, 445–455.

Lindley, P.B., 1979a. Compression module for blocks of soft elastic material bonded to rigid end plates. Journal of Strain Analysis 14, 11–16.

Lindley, P.B., 1979b. Plane strain rotation module for soft elastic blocks. Journal of Strain Analysis 14, 17–21.

Tsai, H.-C., 2003. Flexure analysis of circular elastic layers bonded between rigid plates. International Journal of Solids and Structures 40, 2975–2987.

Tsai, H.-C., 2004. Compression stiffness of infinite-strip bearings of laminated elastic material interleaving with flexible reinforcements. International Journal of Solids and Structures 41, 6647–6660.

Tsai, H.-C., 2005. Compression analysis of rectangular elastic layers bonded between rigid plates. International Journal of Solids and Structures 42, 3395–3410.

Tsai, H.-C., 2006. Compression stiffness of circular bearings of laminated elastic material interleaving with flexible reinforcements. International Journal of Solids and Structures 43, 3484–3497.

Tsai, H.-C., Kelly, J. M., 2001. Stiffness analysis of fiber-reinforced elastomeric isolators. PEER Report 2001/05, Pacific Earthquake Engineering Research Center, University of California, Berkeley.

Tsai, H.-C., Kelly, J.M., 2002a. Stiffness analysis of fiber-reinforced rectangular seismic isolators. Journal of Engineering Mechanics, ASCE 128, 462–470.

Tsai, H.-C., Kelly, J.M., 2002b. Bending stiffness of fiber-reinforced circular seismic isolators. Journal of Engineering Mechanics, ASCE 128, 1150–1157.

Tsai, H.-C., Lee, C.-C., 1998. Compressive stiffness of elastic layers bonded between rigid plates. International Journal of Solids and Structures 35, 3053–3069.

Tsai, H.-C., Lee, C.-C., 1999. Tilting stiffness of elastic layers bonded between rigid plates. International Journal of Solids and Structures 36, 2485–2505.